



Hydrothermal synthesis, structural, electrical and magnetic studies of cathode material $\text{Li}_2\text{FeZrO}_4$ for lithium ion batteries

Viswarupa Mohanty¹ · G. Govindaraj¹

Received: 8 September 2017 / Accepted: 1 December 2017 / Published online: 7 December 2017
© Springer Science+Business Media, LLC, part of Springer Nature 2017

Abstract

In this present work, $\text{Li}_2\text{FeZrO}_4$ has been synthesized by hydrothermal method. The material is characterized using XRD, TGA, FTIR, UV–Vis, VSM and impedance spectroscopy. The powder XRD patterns of $\text{Li}_2\text{FeZrO}_4$ sintered at 800 °C shows that these crystallites are stable in room temperature with tetragonal structure of space group $p141$ and the average crystallites size is found to be 38 nm. Due to its structural stability, ac electrical properties in terms of complex Impedance $Z^*(\omega)$, complex permittivity $\epsilon^*(\omega)$, complex conductivity $\sigma^*(\omega)$ and complex electric modulus $M^*(\omega)$ of the sample have been evaluated as a function of frequency at different temperatures. The shape of the impedance spectra reveals the non-Debye nature of the relaxation processes of the present material. The relaxation process consists of two different polarization processes i.e., hopping charge polarization (“pinned dipole”) and dielectric dipolar like polarization (“free dipole”) mechanism. The dc conductivity activation energy E_σ has been calculated for the material along with the activation energy for hopping conduction and dielectric relaxation. Magnetic properties have been investigated by vibrating sample magnetometer (VSM) for the sample at various temperatures.

1 Introduction

The cathode material of the present study comprises a lithiated zirconium oxide of formula $\text{Li}_2\text{FeZrO}_4$. In recent years, lithium-ion batteries have found to be the most well known energy storage system for consumer and portable electronics [1–4]. The vastly increasing demand for batteries has compelled the scientists and academics to focus on improving the energy densities with a extended range of operating temperatures, durability, safety, charging time and cost of lithium ion battery technology [5–9]. Cathode materials are mostly constructed out of general materials like: LiCoO_2 , LiFePO_4 and LiMn_2O_4 . The cobalt-based cathodes have attracted much attention due to their high theoretical specific heat capacity, high volumetric capacity, low self-discharge, high discharge voltage and good cycling performance [10]. However, along with the high cost of the material, the low thermal stability has become the main drawback. Therefore, for large-scale application, such as electric vehicles and

backup power system, alternating low cost cathode materials, having large faradic capacity are highly desired [10, 11]. From the literatures, it has been found that, a group of alternative cathode materials of lithium rich polyoxyanionic structural compounds [12–15] exhibits distinguishing properties which can be used for large scale Li-ion battery applications. In the present work, we have reported a promising and inexpensive cathode material of the formula $\text{Li}_2\text{FeZrO}_4$. As per the literature survey, a comprehensive study on electrical properties as well as magnetic properties is not available. Recently some workers have reported about the electrochemical properties of $\text{Li}_2\text{FeZrO}_4$ [16]. Hence keeping all the prior things into consideration, an effort has been made in the present work to investigate the ac electrical properties in terms of dc conductivity, electron hopping frequency in electrical quantities, modulus along with permittivity. In this study properly combined conduction and dielectric relaxation functions [17] have been used to analyze the Cole–Cole type relaxation [18] in terms of complex impedance $Z^*(\omega)$, complex permittivity $\epsilon^*(\omega)$, complex conductivity $\sigma^*(\omega)$ and complex electric modulus $M^*(\omega)$ [19, 20] coupling to Jonscher’s idea of ‘pinned dipole’ and ‘free dipole’ [21].

Hydrothermal synthesis is a skilled method for preparation of nano-crystalline materials at low temperature [22]. In the present study, we have focused on the preparation

✉ G. Govindaraj
ggraj_7@yahoo.com

¹ Department of Physics, School of Physical, Chemical and Applied Sciences, Pondicherry University, R.V. Nagar, Kalapet, Pondicherry 605 014, India

and electrical relaxation studies of $\text{Li}_2\text{FeZrO}_4$. Literature survey has confirmed that there is no information available on the synthesis, characterization and electrical properties of the system. The phase composition of $\text{Li}_2\text{FeZrO}_4$ was characterized by X-ray diffraction (XRD) analysis, thermo gravimetric analysis (TGA) and Fourier transform infrared spectroscopy (FTIR). The energy band gap is calculated from UV–Vis spectroscopy analysis. Magnetic properties have been studied through VSM measurements. A detailed study on electrical properties has been discussed in terms of impedance, modulus, conductivity and permittivity. Since there is no dispersive feature below 170 °C in the frequency window of 1–10⁷ Hz, the electrical properties have been carried out in the temperature range of 443–623 K only. The results so achieved have been explained to draw the conclusions, which also have been presented in the study.

2 Experimental details

Hydrothermal synthesis is a unique method to obtain the materials in nano-crystalline forms. Briefly, the basic principle of synthesis method refers to the solubility of inorganic substances in water at exalted temperatures and high pressures, which subsequently forms the crystallization of the dissolved material. In this process, water at elevated temperatures with high pressure plays a crucial role in the precursor material conversion [22].

In the present work, metal nitrates i.e. LiNO_3 , $\text{Fe}(\text{NO}_3)_3 \cdot 9\text{H}_2\text{O}$, $\text{ZrN}_2\text{O}_7 \cdot x\text{H}_2\text{O}$ and sucrose were properly mixed with distilled water in 1:2 molar ratio to get the homogeneous solution. The homogeneous gel was then shifted to teflon lined 100 ml autoclave and heated upto 160 °C for 12 h, resulting the formation of dark brown colored as prepared material. Then the autoclave was cooled to room temperature naturally in air. Furthermore, the resulting materials were cleaned with distilled water and absolute ethanol to get rid of the soluble impurities and depress agglomeration.

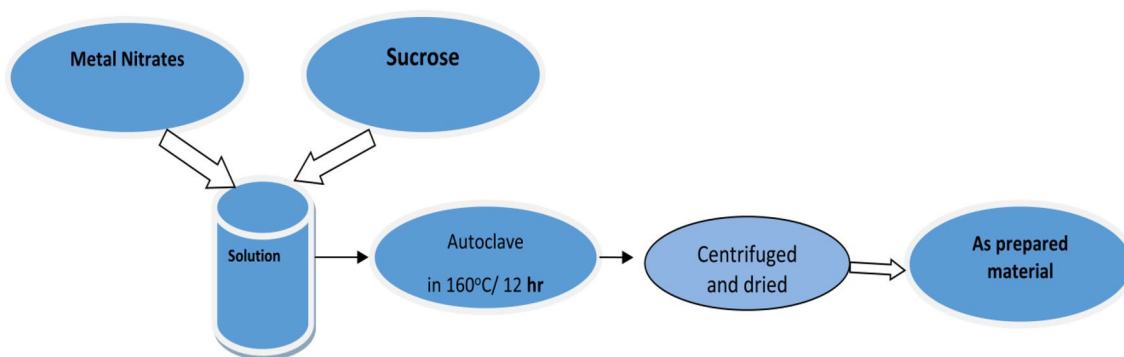


Fig. 1 Schematic diagram for hydrothermal synthesis of the system $\text{Li}_2\text{FeZrO}_4$

After which the product was dried again for 12 h in oven at 80 °C. Further the material was calcined at 800 °C for 12 h for the final product. A schematic diagram of the synthesis procedure is presented in Fig. 1.

The thermal dissipation processes of the as prepared powder were characterized using TG-DTA instrument Model: Q600 SDT from TA instruments under nitrogen flow. The XRD patterns of 800 °C sintered pellets were obtained for the sample using X'pert PANalytical X-ray diffractometer with monochromatic $\text{Cu-K}\alpha$ radiation at glancing angles between the range of 2θ from 20°–80° in a step size of 0.02°. FTIR were recorded using Thermo Nicolet made spectrometer (Model: 6700). The spectrum was recorded between 400 and 4000 cm^{-1} using KBr as the diluting agent. UV–Vis spectrum was measured using Ocean optics HR4000 in the range 300–800 nm. VSM studies were carried out by using Physical property measurement system (PPMS Evercool II) from Quantum design model no- PM 872. Before carrying out the electrical measurements, the prepared pellets were calcined at 800 °C for 12 h. The parallel and opposite sides of the pellets were coated with silver paint to have good ohmic contact and also to make parallel plate capacitor geometry with the material as a dielectric medium. The electrical properties were measured with a Material Mates Impedance Analyzer 7260, in the temperature range of 443–623 K in the step size of 20 K, which gives the real and the imaginary part of the impedance covering the frequency range of 1–10⁷ Hz.

3 Results and discussion

3.1 X-ray diffraction studies

Figure 2 shows the XRD patterns of $\text{Li}_2\text{FeZrO}_4$ sintered at 800 °C. The sample shows the most sharp and intense peak (200), which confirms the formation of crystalline structure. The results obtained by XRD are indexed using JCPDS

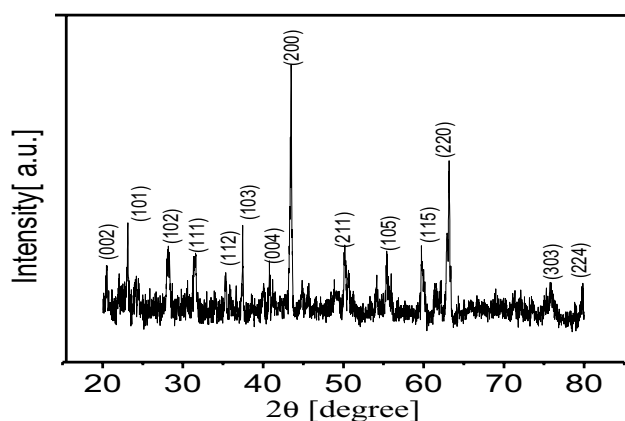


Fig. 2 XRD pattern of $\text{Li}_2\text{FeZrO}_4$ sintered at $800\text{ }^\circ\text{C}$

reference code 38-0281. The phase pure crystallites are found to be having stable tetragonal crystal structure with space lattice P -type and lattice parameters, $a=4.1988\text{ \AA}$ and $c=9.0607\text{ \AA}$ which is matching with the values reported earlier by Mandal et al. [16]. Hence the average crystallite size is calculated using Scherrer's formula:

$$t = 0.9\lambda / \beta \cos\theta$$

where λ is the wavelength of the Cu- K_α radiation ($\lambda=1.5418\text{ \AA}$) and β is the integral width in radians [11]. The crystallite size of $800\text{ }^\circ\text{C}$ calcined materials is obtained to be approximately 38 nm .

3.2 Thermo gravimetric analysis

As prepared sample was analysed by thermal gravimetric analysis (TGA). Figure 3 demonstrates the TGA result conducted on the powder of as prepared samples under nitrogen

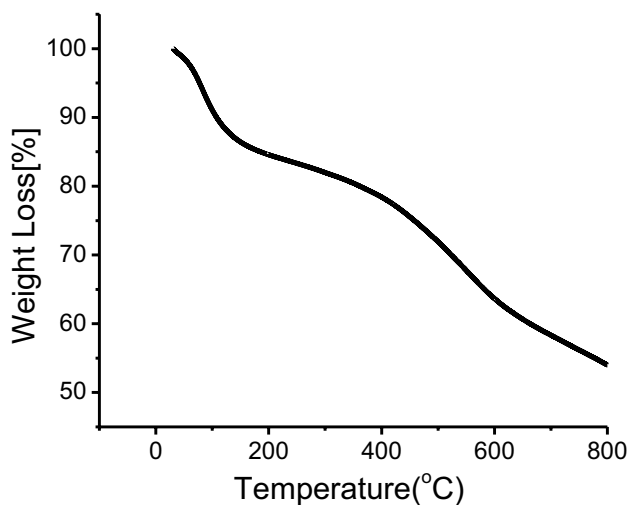


Fig. 3 Typical thermogram for $\text{Li}_2\text{FeZrO}_4$

flow. The analysis of TG data shows three obvious mass losses with a total weight loss of 45%. A weak mass loss of around 10% is observed before $150\text{ }^\circ\text{C}$ due to the evaporation of water vapors. In the second step of weight loss, the weight loss is around 20% ascribed to the decomposition of organic fuel/complexing agent and nitrates at $400\text{--}600\text{ }^\circ\text{C}$. In the third step, weight loss is found to be around 10% due to phase formation of the material at $650\text{ }^\circ\text{C}$ because of decomposition of nitrates into oxides. That means that the material develops a stable phase after heating above $650\text{ }^\circ\text{C}$.

3.3 Fourier transform infrared spectroscopy studies

Study of infrared absorption spectra provides the information about position of ions in the crystal lattice along with the vibrational spectra [23]. Figure 4 shows the FTIR spectra of $\text{Li}_2\text{FeZrO}_4$ system in the range $400\text{--}2000\text{ cm}^{-1}$. The observed FTIR peak in the region $400\text{--}765\text{ cm}^{-1}$ refers to the internal vibrations of metal ion and oxygen bonds in the unit cell. The Li atoms are located in octahedra environment of LiO_6 and vibrational modes of Li–O are observed at 412 and 449 cm^{-1} [12]. The absorption bands at $498\text{--}523\text{ cm}^{-1}$ correspond to Zr–O vibrations [24]. The band $546\text{--}709\text{ cm}^{-1}$ corresponds to $\text{Fe}^{3+}\text{--O}^{2-}$ vibration [11, 25]. The prominent peak at 1452 cm^{-1} region refers to O=H bonding and peak in the region of 1550 cm^{-1} , signifies to the adsorbed moisture [26].

3.4 UV–Vis spectroscopy studies

Optical absorption measurements are extensively used to demonstrate the electronic properties of the material by determining the band gap energy. The UV spectrum exhibits

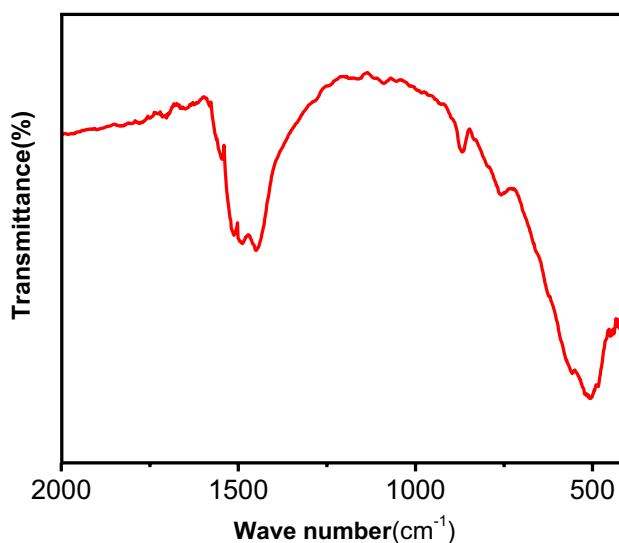


Fig. 4 FTIR spectra of $\text{Li}_2\text{FeZrO}_4$ material sintered at $800\text{ }^\circ\text{C}$

a broad absorption edge around 485 nm which occurs due to the electronic transition from valence to conduction band.

The absorption coefficient (α) of the nano-crystallites has been determined using the fundamental relationships [27, 28].

$$I = I_0 e^{-\alpha t}$$

$$A = \log(I/I_0),$$

$$\alpha = 2.303(A/t), \quad (1)$$

where A is the absorbance and t is the thickness of the sample in cm. To evaluate the direct band gap energy for the sample, the graph of $(\alpha h\nu)^2$ versus $h\nu$ has been plotted. The optical band gap energy was calculated from the absorption spectra by extrapolating the linear portion of the graph between to the energy axis using Tauc's relation [29–33] as shown in Fig. 5a, b. The Tauc's expression is given by following equation.

$$\alpha h\nu = B(h\nu - E_g)^{1/2} \quad (2)$$

where E_g is average band gap energy of the material and B is band tailing parameter [34]. Value of band gap energy, absorption coefficient α and constant B can be obtained from the intercept of the line at $\alpha=0$. The band gap was found to be approximately 2.7 eV.

3.5 AC electrical studies

The electrical properties of ion/electron conducting materials play an important role and often decide about the application of the material for a particular device. With the passing of ac electric current through a solid electrolyte, various processes are observed which includes ion movement through the electrolyte and transfer of charge across the electrode–electrolyte interface. Each process respond to the applied ac electric field in different frequency ranges because of the different relaxation times associated with the process. Experimental complex impedance data mainly refers to the impedance of an equivalent circuit consisting of various resistors, capacitors and different involved elements in the circuits. These equivalent circuits can be accredited to the process consisting of the resistance (R) and the constant phase element (CPE) combined in series and parallel. The real $Z'(\omega)$ and the imaginary $Z''(\omega)$ of the complex impedance $Z^*(\omega)$ are directly measured from the instrument Materials Mates 7260 Impedance Analyzer.

From the very beginning of Cole and Cole [18] to recent time period, dielectric behaviour and electrical conductivity of solid state materials has been analyzed in utilizing complex plane plots and frequency explicit plots [35]. The real $Z'(\omega)$ and the imaginary $Z''(\omega)$ parts of the complex impedance $Z^*(\omega)$ has been calculated by using the relations given below

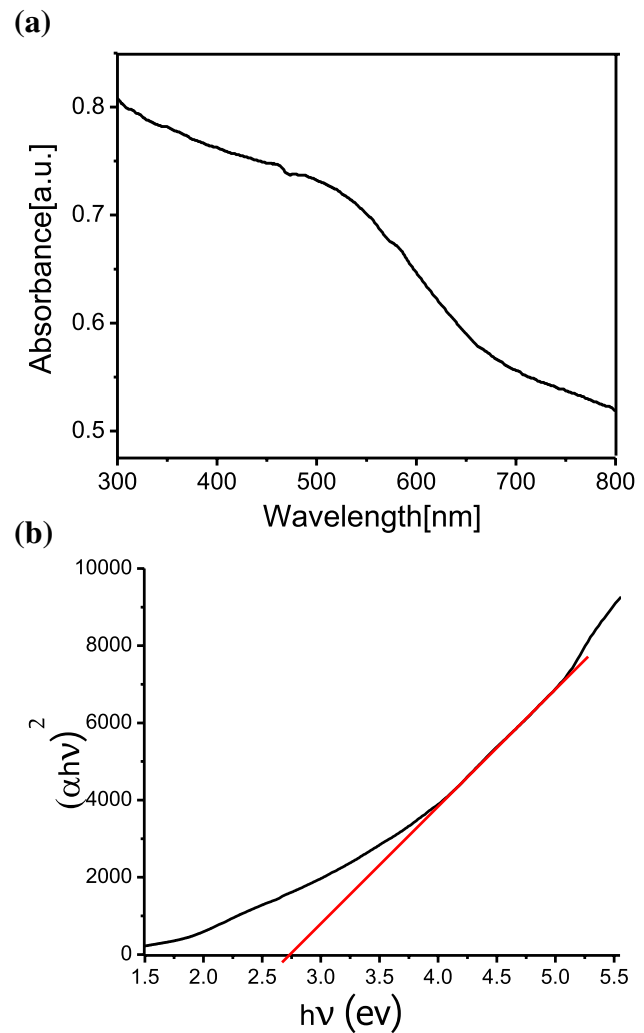


Fig. 5 **a** The UV–Vis spectrum of the $\text{Li}_2\text{FeZrO}_4$ material sintered at 800 °C, **b** Tauc plot for dependence of $(\alpha h\nu)^2$ on photon energy ($h\nu$)

$$Z'(\omega) = G/(G^2 + \omega^2 C^2), \quad (3)$$

$$Z''(\omega) = C\omega/(G^2 + \omega^2 C^2), \quad (4)$$

where G and C are the measured parallel conductance and the capacitance and angular frequency, $\omega = 2\pi f$, f being the frequency [18].

The electrical properties of an ion/electron conductor can be explained by an equivalent circuit which consists of a parallel combination of a resistor R and a capacitor C . The complex impedance plot of this circuit demonstrates a semicircle whose centre lies on the real axis. However, in most of the cases the experimental data comprises of a depressed semicircle in complex impedance plot which is a deviation from simple R – C circuit plot in parallel. A

common way to describe these depressed semicircles is through a parallel combination of a resistor R and a constant phase element (CPE) [36].

In case of parallel R –CPE circuit, the equivalent impedance can be written as:

$$Z_{equiv} = Z_R Z_{CPE} / (Z_R + Z_{CPE}), \quad (5)$$

where $Z_R = R$. The impedance Z_{CPE} can be represented by $Z_{CPE} = 1/Y_0(j\omega)^n$, Y_0 and n are parameters which are usually temperature dependent but independent of frequency [37] and the value of n lies in $0 < n < 1$. In case of $n = 1$ the CPE works as an ideal capacitor where as $n = 0$ refers to a simple resistor. In case of $0 < n < 1$, the value of CPE is a combination of resistance and capacitance. The CPE is predominantly used to describe the distribution of the value of some physical property of the system along with non-Debye process [38, 39].

Generally, for the investigation of ac impedance data, an electrically equivalent circuit containing R and CPE combination in parallel is considered. The equivalent circuit modeled by Cole–Cole function, is as follows:

$$Z^* = R / [1 + (j\omega\tau)^{1-\alpha}] \quad (6)$$

where $\tau = RC$ and $0 \leq \alpha < 1$ implies the distribution of the relaxation times. But in case of ideal Debye relaxation, $\alpha = 0$. But in this present study, combination of ‘pinned dipole’ and ‘free dipole’ relaxation have been taken into account considering the material posses relaxation due to both the relaxation processes with the application of ac electric field. Recently, Kumar et al. [17] have reported about combined conduction and dielectric relaxation formalism considering the combined ‘pinned dipole’ and ‘free dipole’ relaxation. According to the formalism, pinned dipole’ relaxation time τ_c is relevant to conduction process where as ‘free dipole’ relaxation time τ_d is refers to dielectric process. The relation of dc conductivity with τ_c and τ_d demonstrates the dynamics of combination of ‘pinned dipole’ and ‘free dipole’. The obtained physical parameters of ‘pinned dipole’ and ‘free dipole’ formalism are unique for all representations like $Z^*(\omega)$, $\epsilon^*(\omega)$, $\sigma^*(\omega)$ and $M^*(\omega)$. According to the formalism, a reduced field effect is produced due to the alignment of ‘free dipoles’ in the direction of the applied field. Simultaneously, when a free charge carrier jumps from a site to another site, it involves a slow rate of transfer of charge creating the time dependent polarization during transition, which alternately produces a ‘pinned dipole’ i.e. a pinned dipole can be assigned to hopping of free charge and ion lattice [20, 21].

In the case of anomalous relaxation, a combination of conduction and dielectric process with Cole–Cole type distribution of relaxation time is taken into consideration and thus complex permittivity is derived by Kumar et al. [17] as:

$$\epsilon^*(\omega) = \frac{\sigma_{dc}(1 + (i\tau_c\omega)^{\alpha_c})}{i\omega\epsilon_0} + \frac{\epsilon_d}{1 + (i\omega\tau_d)^{\alpha_d}} + \epsilon_\infty \quad (7)$$

Henceforth complex conductivity of the combined ‘pinned dipole’ and ‘free dipole’ is obtained as [17],

$$\sigma^*(\omega) = \sigma_{dc}(1 + (i\tau_c\omega)^{\alpha_c}) + i\omega\epsilon_0 \left(\epsilon_\infty + \frac{\epsilon_d}{1 + (i\omega\tau_d)^{\alpha_d}} \right) \quad (8)$$

where $\sigma^*(\omega)$ stands for total complex conductivity, σ_{dc} stands for DC conductivity, α_c is Cole–Cole exponent of conduction relaxation, $0 < \alpha_c < 1$, α_d is Cole–Cole exponent of dielectric relaxation, $0 < \alpha_d < 1$. Again the complex resistivity is obtained as,

$$\rho^*(\omega) = \frac{1}{\sigma_{dc}(1 + (i\tau_c\omega)^{\alpha_c}) + i\omega\epsilon_0 \left(\epsilon_\infty + \frac{\epsilon_d}{1 + (i\omega\tau_d)^{\alpha_d}} \right)} \quad (9)$$

as $\rho^*(\omega) = 1/\sigma^*(\omega)$ which signifies the predominant resistivity of parallel combination of the Cole–Cole type dielectric and conductivity relaxation [17].

Figure 6 shows ac electrical data of the sample in different representations (a) $Z''(\omega)$, (b) $M''(\omega)$, (c) $\epsilon''(\omega)$ and (d) $\sigma'(\omega)$ with fitted curve for various temperatures. All the representations show a good compliance with the electrical parameters shown in Table 1. The equivalent circuit used in analysis of the relaxation process [17] is given as inset of Fig. 6a(i). The peak which is exhibited by Z'' shifts towards higher frequencies side with increasing temperature. The curves are asymmetric and broader than the usual nature of Debye curve [37]. These features reveals that the pinned dipole relaxation time τ_c is not single valued which is distributed discretely around a mean [37] $\tau_m = 1/\omega_c$ i.e. the distribution varies with temperature variance. With the increase of temperature, the magnitude of Z'' peak maxima decreases along with the shift of peak frequency towards the higher temperature side [38, 39]. Solids lines in Fig. 6a–d, are the fitted curves to the experimental results according to Eq. (9). It is obvious from the figures that the experimental data and fitting agrees consistently in the total range of frequencies and the same parameter consistently fit the data in all other representations. Ac electrical data of $\text{Li}_2\text{FeZrO}_4$ in $Z''(\omega)$, $M''(\omega)$, $\epsilon''(\omega)$ and $\sigma'(\omega)$ at temperature 563 K is shown in Fig. 7.

Due to ‘free dipole’ relaxation mechanism, after the cross over frequency, conductivity $\sigma'(\omega)$ is affected and thus deviates from the natural power law behavior. From the conductivity plot shown in Fig. 6d, it has been found out that a systematic decrease of dc conductivity happens with an increase of temperature. This confirms that the nature of

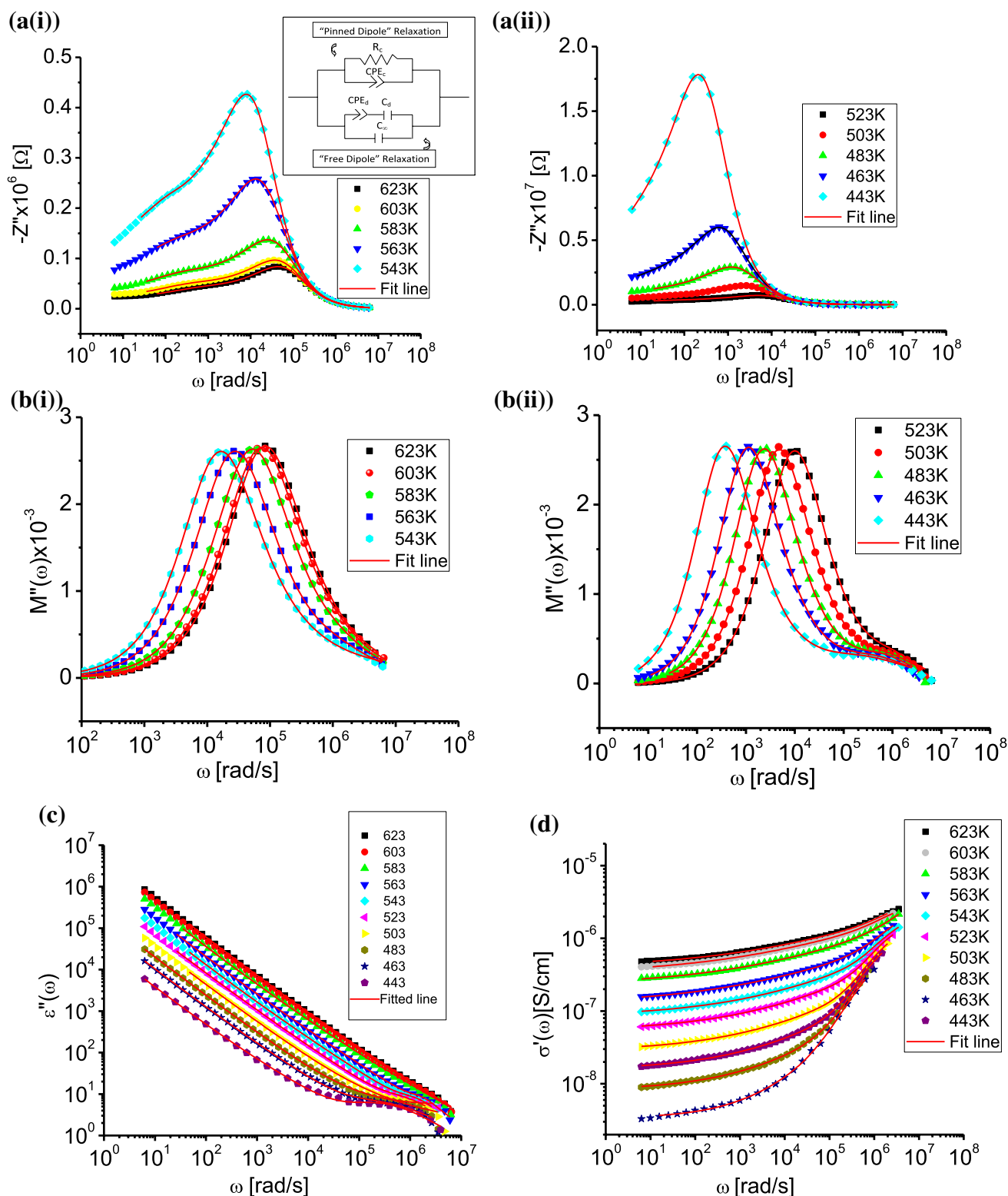


Fig. 6 Complex impedance data of $\text{Li}_2\text{FeZrO}_4$ in different representations **a(i)**, **(ii)** $Z''(\omega)$, **b(i)**, **(ii)** $M''(\omega)$, **c** $\epsilon''(\omega)$ and **d** $\sigma'(\omega)$ ac representations, the parameters extracted (Table 1) from the complex impedance analyses were used

used for fitting of data). In **b** $M''(\omega)$, **c** $\epsilon''(\omega)$ and **d** $\sigma'(\omega)$ ac representations, the parameters extracted (Table 1) from the complex impedance analyses were used

Table 1 Physical parameters extracted from fitting of conduction and dielectric relaxation of $\text{Li}_2\text{FeZrO}_4$ at different temperatures

T (K)	Conduction relaxation			Dielectric relaxation			
	σ_{dc} (S/cm)	τ_c (s)	α_c	τ_d (s)	α_d	ϵ_d	ϵ_∞
623	$(4.067 \pm 0.012) \times 10^{-7}$	$(9.82 \pm 0.5) \times 10^{-5}$	0.240 ± 0.003	$(1.51 \pm 0.1) \times 10^{-3}$	0.843 ± 0.022	440.01 ± 23.26	146.30 ± 0.47
603	$(3.409 \pm 0.012) \times 10^{-7}$	$(1.18 \pm 0.1) \times 10^{-4}$	0.237 ± 0.005	$(3.57 \pm 0.5) \times 10^{-3}$	0.781 ± 0.025	604.27 ± 45.12	146.20 ± 0.45
583	$(2.364 \pm 0.008) \times 10^{-7}$	$(2.13 \pm 0.1) \times 10^{-4}$	0.248 ± 0.002	$(5.03 \pm 0.7) \times 10^{-3}$	0.814 ± 0.025	661.99 ± 23.21	145.30 ± 0.42
563	$(1.272 \pm 0.002) \times 10^{-7}$	$(4.28 \pm 0.1) \times 10^{-4}$	0.251 ± 0.001	$(6.05 \pm 0.3) \times 10^{-3}$	0.853 ± 0.011	409.46 ± 14.24	146.88 ± 0.37
543	$(7.917 \pm 0.092) \times 10^{-8}$	$(6.44 \pm 0.9) \times 10^{-4}$	0.260 ± 0.003	$(8.76 \pm 0.2) \times 10^{-3}$	0.960 ± 0.069	264.95 ± 14.34	146.54 ± 0.57
523	$(4.869 \pm 0.051) \times 10^{-8}$	$(1.39 \pm 0.5) \times 10^{-3}$	0.259 ± 0.004	$(1.60 \pm 0.2) \times 10^{-2}$	0.853 ± 0.021	318.48 ± 29.42	147.78 ± 0.68
503	$(2.592 \pm 0.021) \times 10^{-8}$	$(3.71 \pm 0.7) \times 10^{-3}$	0.274 ± 0.004	$(3.10 \pm 0.1) \times 10^{-2}$	0.931 ± 0.020	331.11 ± 19.45	147.63 ± 0.73
483	$(1.411 \pm 0.034) \times 10^{-8}$	$(7.42 \pm 0.2) \times 10^{-3}$	0.296 ± 0.010	$(9.68 \pm 0.3) \times 10^{-2}$	0.836 ± 0.031	456.99 ± 29.37	144.83 ± 0.99
463	$(6.291 \pm 0.3) \times 10^{-9}$	$(2.38 \pm 0.5) \times 10^{-2}$	0.158 ± 0.020	$(1.28 \pm 0.2) \times 10^{-1}$	0.622 ± 0.060	531.24 ± 24.31	146.23 ± 0.62
443	$(2.598 \pm 0.1) \times 10^{-9}$	$(3.34 \pm 0.2) \times 10^{-2}$	0.297 ± 0.034	$(3.37 \pm 0.7) \times 10^{-1}$	0.680 ± 0.051	539.03 ± 19.75	144.60 ± 0.76

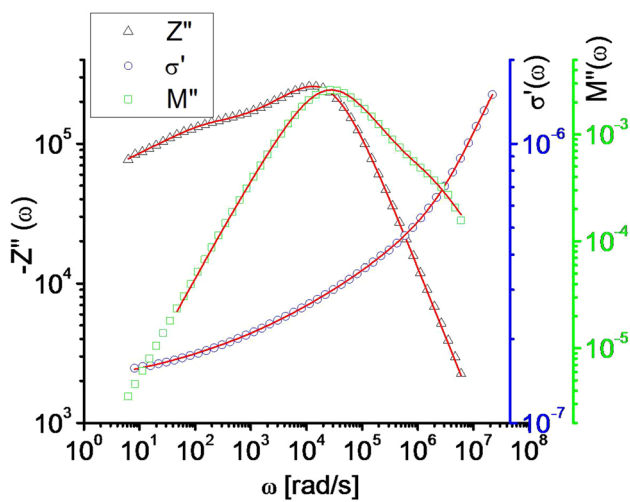


Fig. 7 Ac electrical data of conduction relaxation and dielectric relaxation of $\text{Li}_2\text{FeZrO}_4$ at temperature 563 K with fit curve with $Z''(\omega)$, $M''(\omega)$ and $\sigma'(\omega)$ representations

the material is semi-conductor type. Generally conductivity followed by Arrhenius law is presented by

$$\sigma_{dc} T = \sigma_0 \exp[-E_\sigma/k_B T] \tag{10}$$

where σ_0 is pre-exponential factor and E_σ gives the conduction activation energy. The Arrhenius plot for dc conductivity at various temperatures of the material is presented in Fig. 8a. Thus obtained activation energy E_σ for $\text{Li}_2\text{FeZrO}_4$ is found to be 0.63 ± 0.02 eV.

Due to thermally activated nature of distributed pinned dipole relaxation time τ_c , it follows the Arrhenius relation which is given in Eq. (11)

$$1/\tau_c = (1/\tau_0) \exp[-E_c/k_B T] \tag{11}$$

where $1/\tau_0$ refers to the attempted jump of charge carriers inside the material with activation energy E_c . Thus the

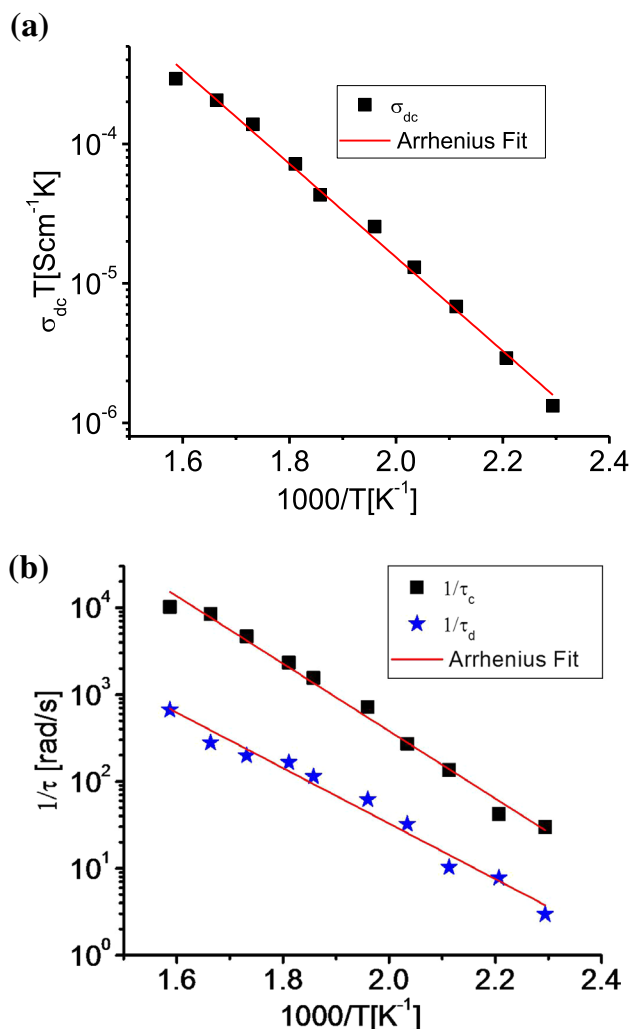


Fig. 8 The Arrhenius behavior of **a** dc conductivity, **b** conduction relaxation time τ_c and dielectric relaxation time τ_d for $\text{Li}_2\text{FeZrO}_4$

activation energy related to hopping motion is found to be 0.73 ± 0.02 eV calculated from the linear fit of Fig. 8b. A relaxation peak observed in dielectric loss $\varepsilon''(\omega)$ is dominated by the contribution of dc conduction part with elevation of temperature. But in some other reported materials the effects of dielectric relaxation are seen at high frequencies [40, 41]. In the present study, electric modulus $M''(\omega)$ possesses two relaxation processes ascribing to the ‘pinned dipole’ relaxation relevant to conduction process and ‘free dipole’ relaxation referring to dielectric process.

In this concept, the parameter ‘ α_d ’ is ascribed as the nature of the obtained symmetrical broadening of dielectric loss peak. It conveys the symmetrical distribution of relaxation time of free dipole with respect to τ_d where the distribution is weakly temperature dependent. The free dipole relaxation time τ_d for different temperatures is presented in Fig. 8b which follows Arrhenius behaviour due to its thermally activated nature as

$$1/\tau_d = (1/\tau_\infty) \exp[-E_d/k_B T] \quad (12)$$

where k_B and T refers to is the Boltzmann constant and absolute temperature respectively, whereas τ_∞ refers to the relaxation time at infinite temperature. Here activation energy due to ‘free dipole’ is found to be 0.60 ± 0.02 eV.

3.6 Vibrating sample magnetometer studies

To understand the magnetic behaviour of $\text{Li}_2\text{FeZrO}_4$ particles, M – H loops at different temperature range 10–300 K and temperature dependent magnetic properties under ZFC and FC conditions over a range of temperatures 10–300 K were carried out on the sample. Figure 9a displays M – H loops and variations of magnetization obtained at 20 kOe. During the starting of magnetization process, the lower-field region shows the significant increase of magnetization with increasing applied magnetic field. However, with further increase of magnetic field, increase of magnetization delayed. Finally, with increasing magnetic field the magnetization increases almost linearly and thus saturation is not obtained. These results suggest that there are two components associated with the magnetization reversal process [42]: (i) at low-field region, magnetizing component responsible for weak ferromagnetic property and (ii) in high-field region, a non-saturating component responsible for the consistent linear variation which indicates a anti-ferromagnetic behavior.

The zero field cooled–field cooled (ZFC–FC) curves in the range of 10–300 K are shown in Fig. 9b. The FC curve demonstrates a broad split with the increasing magnetization values till 10 K. This behaviour indicates the presence of the anti-ferromagnetic property below 50 K [43] which can be correlated from the M – H loop obtained at 10 K. From the curve, it is clear that the material has Neel transition (T_N) temperature of 48 K and below this temperature, it is reported to have ordering of anti-ferromagnetic nature [44].

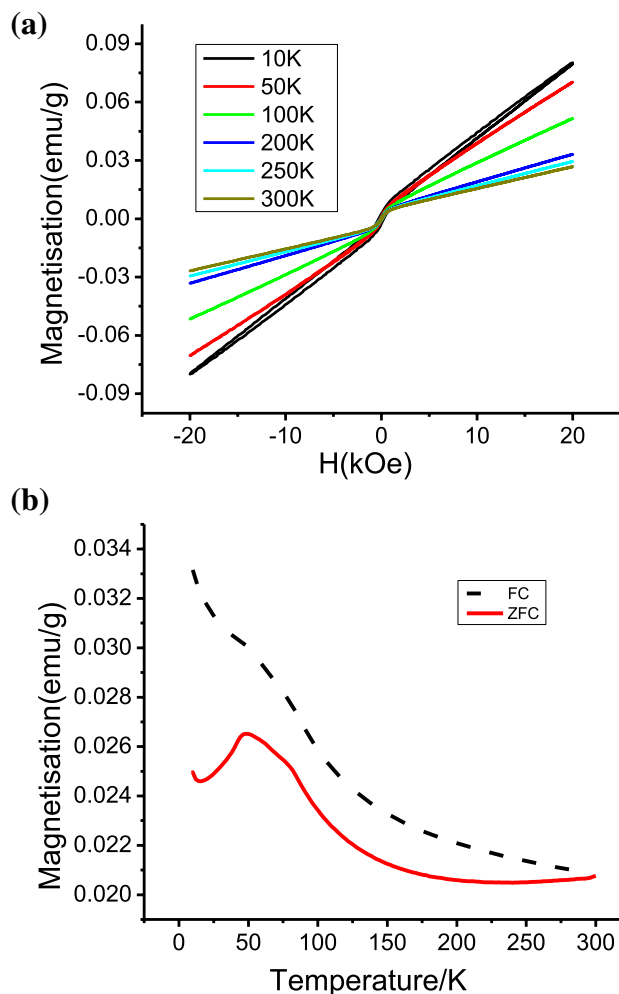


Fig. 9 **a** M – H Loop at different temperatures of the system. **b** Low temperature M – T curves measured under ZFC and FC conditions for $\text{Li}_2\text{FeZrO}_4$

4 Conclusions

A lithiated Zirconium oxide of the formula $\text{Li}_2\text{FeZrO}_4$ was successfully prepared by well-known hydrothermal synthesis method. XRD results revealed about the crystalline nature of the materials having tetragonal structure. From the optical analysis, the band gap energy is calculated to be approximately 2.7 eV. The electrical studies have been carried out in terms of representations of $Z''(\omega)$, $M''(\omega)$, $\varepsilon''(\omega)$ and $\sigma'(\omega)$ for various temperatures and the data were fitted to the Cole–Cole anomalous fitting considering the involvement of pinned dipole and free dipole relaxation. The shape of the imaginary part of the modulus suggests that there are two relaxation processes in the material which refers to pinned dipole and free dipole relaxation mechanism. The nature of relaxation processes is confirmed to be non-Debye. The E_σ , E_c and E_d value has been obtained from impedance analysis. The dc conductivity

activation energy is found to be 0.63 eV, where as the cross over frequency activation energy for the pinned dipole is found to be 0.70 eV and activation energy for free dipoles is found to be 0.60 eV for $\text{Li}_2\text{FeZrO}_4$. Along with this, the magnetic studies reveal that the material shows anti-ferromagnetic behaviour with very low ferromagnetic nature.

Acknowledgements Financial support from UGC-SAP F.03(1279)/13/EMR-II is gratefully acknowledged. Authors would like to thank Central Instrumentation Facility (CIF), Pondicherry University for TGA, UV–Vis and VSM facilities.

References

- M. YazidSaidi, J. Barker, R. Koksbang, United States Patent, Patent Number: 6,103,419. dop; Aug.15,2000/US006103419A
- A.K. Padhi, K.S. Nanjundaswamy, J.B. Goodenough, *J. Electrochem. Soc.* **144**, 1188–1194 (1997)
- M. Jo, Y.K. Lee, K.M. Kim, J. Cho, *J. Electrochem. Soc.* **157**, A841–A845 (2010)
- M.M. Thackeray, in *Programme, Batteries. Battery material, Lithium Ion Battery Technology*, vol. 141, ed. by R.T. Brodd (ITEJES Press, OH, 1995), p. 1
- M.D. Levi, K. Gamolsky, D. Aurbach, U. Heider, R. Oesten, *J. Electrochem. Soc.* **147**, 25–33 (2000)
- Y.K. Sun, Y.S. Jeon, *J. Mater. Chem.* **9**, 3147–3150 (1999)
- Y.K. Sun, *Electrochem. Commun.* **2**, 6–9 (2000)
- T. Omura, T. Kodera, T. Ogihara, *J. Ceram. Soc. Jpn.* **123**, 280–284 (2015)
- K. Suryakala, G. Paruthimal Kalaignan, T. Vasudevan, *Int. J. Electrochem. Sci.* **1**, 372–378 (2006)
- L. Vijayan, R. Cheruku, G. Govindaraj, *J. Appl. Phys.* **111**, 064905 (2012)
- V. Mohanty, R. Cheruku, L. Vijayan, G. Govindaraj, *J. Mater. Sci. Technol.* **30**, 335–341 (2014)
- R. Cheruku, L. Vijayan, G. Govindaraj, *Mater. Sci. Eng. B* **177**, 771–779 (2012)
- M. Castellanos, M.C. Martinez, A.R. West, *Z. Kristallogr.* **190**, 161 (1990)
- L. Sebastian, J. Gopalakrishnan, *J. Solid State Chem.* **172**, 171–177 (2003)
- M.V.V.M. Satya Kishore, S. Marinel, V. Pralong, V. Caignaert, S. D’Astorg, B. Raveau, *Mater. Res. Bull.* **41**, 1378–1384 (2006)
- I. Bikash Mandal, S. Basumallick, Ghosh, *Adv. Mater. Lett.* **7**, 150–155 (2016)
- N.S.K. Kumar, T.S. Shahid, G. Govindaraj, *Phys. B* **488**, 99–107 (2016)
- K.S. Cole, R.H. Cole, *J. Chem. Phys.* **9**, 341–351 (1941)
- J.C. Dyre, *J. Appl. Phys.* **64**, 2456–2468 (1988)
- D.L. Sidebottom, *Rev. Mod. Phys.* **81**, 999–1014 (2009)
- A.K. Jonscher, *Nature* **253**, 717–719 (1975)
- O. Schäf, H. Ghobarkar, P. Knauth, in *Nanostructured Materials, Part of the Electronic Materials: Science & Technology*, vol. 8, ed. by P. Knauth, J. Schoonman (Springer, New York, 2002), pp. 23–41
- S. Sorokhaibam, I. Soibam, S. Phanjoubam, *Int. J. Adv. Sci. Eng. Technol.* **4**, 120–122 (2016)
- D. Sarkar, D. Mohapatra, S. Ray, S. Bhattacharyya, S. Adaka, N. Mitra, *Ceram. Int.* **33**, 1275–1282 (2007)
- Y. Luo, L. Liu, W. Qiao, F. Liu, Y. Zhang, W. Tan, G. Qiu, *Mater. Chem. Phys.* **170**, 239–245 (2016)
- A.K. Singh, U.T. Nakate, *Sci. World J.* **2014**, 1–7 (2014)
- S. Singhal, S. Bhukal, J. Singh, K. Chandra, S. Bansal, *J. Nanotechnol.* **2011** (2011)
- M. Srivastava, A.K. Ojha, S. Chaubey, A. Materny, *J. Alloys Compd.* **481**, 515–519 (2009)
- S.K. O’Learly, P.K. Lim, *Solid State Commun.* **104**, 17–21 (1997)
- R. Kumar, P. Singh, *Res. Phys.* **3**, 122–128 (2013)
- J. Podder, S. Sagadevan, I. Das, *J. Mater. Sci. Mater. Electron.* **27**(6), 5622–5627 (2016)
- F. Urbach, *Phys. Rev.* **92**, 1324 (1953)
- S. Adachi, *Optical Properties of Crystalline and Amorphous Semiconductors: Materials and Fundamental Principles*, 1st edn. (Kluwer Academic Publishers, Boston, 1999), pp. 207–208
- H.S. Metwally, *Acta Phys. Pol. A* **99**, 683–690 (1991)
- R. Gerhardt, *J. Phys. Chem. Solids* **55**, 1491–1506 (1994)
- R.S.T.M. Sohn, A.A.M. Macêdo, M.M. Costa, S.E. Mazzetto, A.S.B. Sombra, *Phys. Scr.* **82**, 055702 (2010)
- E. Barsoukov, J. Ross Macdonald (eds.), *Impedance Spectroscopy, Theory and Applications* (Wiley, New York, 2005)
- P. Maass, J. Petersen, A. Bunde, W. Dieterich, H.E. Roman, *Phys. Rev. Lett.* **66**, 52–55 (1991)
- B. Roling, C. Martiny, S. Bruckner, *Phys. Rev.* **B63**, 214203 (2001)
- N.S.K. Kumar, T.S. Shahid, G. Govindaraj, *Int. J. Chem. Technol. Res.* **6**, 2213–2215 (2014)
- R. Murugraj, G. Govindraj, D. George, *J. Mater. Sci.* **37**, 5101–5106 (2002)
- B. Kisan, P. Ravikumar, A. Das, A. Srinivasan, A. Perumal, *Sci. Lett. J.* **4**, 160 (2015)
- K. Saravana Kumar, C. Venkateswaran, *IOP Conf. Ser. Mater. Sci. Eng.* **73**, 012031 (2015)
- F. Huang, Z. Wang, X. Lu, J. Zhang, K. Min, W. Lin, R. Ti, T.T. Xu, J. He, C. Yue, J. Zhu, *Sci. Rep.* **3**, 2907 (2013)